Journal of Computational Mathematics
Vol.xx, No.x, 2025, 1–15.

http://www.global-sci.org/jcm
doi:10.4208/jcm.2503-m2024-0010

AN ADAPTIVE ALGORITHM FOR L1-FIDELITY COLOR IMAGE RESTORATION*

Wei Wang [1)], Chengyun Yang and Qifan Song
School of Mathematical Sciences, Key Laboratory of Intelligent Computing and Applications (Ministry of Education), Tongji University, Shanghai 200092, China
Emails: wangw@tongji.edu.cn, 2211185@tongji.edu.cn, 2030928@tongji.edu.cn

Abstract

In this paper, we propose an adaptive algorithm for L1-fidelity color image restoration by using saturation-value total variation. The main contribution of this paper is to employ the generalized cross validation method efficiently and automatically to estimate the regularization parameter in a saturation-value total variation plus L1-fidelity color image restoration model. We consider Poisson noise and mixed noise in this paper, and the experimental results show that the visual quality and the SSIM/PSNR/SAM values of the restored images by using the proposed algorithm are competitive with other tested existing methods, which makes the proposed algorithm to be comparable both quantitatively and qualitatively.

Mathematics subject classification: 65J22, 65K10, 68U10.
Key words: Adaptive algorithm, Saturation-value total variation, L1-fidelity, Cross validation, Poisson noise.

1. Introduction

Image restoration is a crucial task in image processing because real images are often corrupted by factors such as noise, dust, and scratches that reduce the effectiveness of other image processing activities like segmentation and pattern recognition. One of the critical issues associated with image restoration is image denoising, which entails reducing noise in digital images obtained from diverse imaging systems such as cameras, scanners, microscopes, and telescopes. The four main types of noise that occur in digital images are Gaussian, Poisson, impulse, and mixed Gaussian-Poisson noise. Poisson noise is especially prevalent in low-light conditions, resulting in grainy or speckled images, which can be represented as a Poisson distribution that describes the probability of detecting a certain number of photons over a given time or area. Various techniques such as smoothing filters [30,31] or denoising algorithms [17,32] that utilize the statistical properties of noise can be employed to reduce Poisson noise.

In this paper, we focus on variational methods. As we know that L2-fidelity does not give satisfactory results when dealing with non-Gaussian noise. Several non-smooth data-fitting terms such as L1-norm have been extensively studied for dealing with non-Gaussian noise including impulse noise, Poisson noise, etc. Chan and Esedoglu [6] further studied non-smooth fidelity for image restoration with respect to non-Gaussian noise. The total variation regularization plus L1-fidelity (TV-L1) model has been studied in the literature, e.g. the connection with

* Received January 15, 2024 / Revised version received December 3, 2024 / Accepted March 7, 2025 / Published online May 29, 2025 /
[1)] Corresponding author

mathematical morphology [7], applications in impulse noise removal [23,25], cartoon-texture decomposition [1,5,13,29], etc. In 1998, Blomgren and Chan [2] proposed a color total variation (CTV_1) regularization model by using a global channel coupling which is specifically considering the L2-norm of each channel's total variation. Bresson and Chan [3] proposed CTV_2 model which is a local channel coupling by considering the L2-norm of all channels' derivations locally. J. Duran *et al.* [9] pointed out that CTV_1 is good at color image restoration under similar noise in each channel, and CTV_2 can determine edge locations in different channels due to its stronger channel coupling. Liu *et al.* [20] presented a hybrid model that combines the TV regularizer and the high-order TV regularizer with L1 data-fitting term (HTV-L1) for salt-and-pepper impulse noise removal. High-order TV regularizer can effectively suppress the occurrence of staircase effects. The Framelet transform is regarded as a regularization term that uses wavelets for image processing [4,8,24]. Dong *et al.* [8] presented two framelet-based regularization approaches employing L1-fidelity for blind image inpainting and other applications, such as random-valued impulse noise removal. Saturation-value total variation (SVTV) is designed for color image processing, which considers the channel coupling based on quaternion framework. SVTV has been proved to be very effective for color image recovery [16]. Wang and Song [27] developed SVTV-L1 model for Poisson noise removal by introducing saturation-value total variation as a regularizer and the L1-norm as a data-fitting term in the energy functional.

In the variational model, the regularization parameters must be determined properly so that the numerical algorithms can be used to provide good recovered images. The above-mentioned models [27] do not give an efficient method for searching suitable regularization parameters. Generalized cross-validation (GCV) [12] is a rotation-invariant version of the ordinary cross-validation, and is usually used to find a good ridge parameter, e.g. automatic deblurring [22,26], image denoising [18], learning based systems [11], etc. The main contribution of this paper is to employ the generalized cross validation (GCV) method efficiently and automatically to estimate the regularization parameter associated with the priors in SVTV-L1 model for color image restoration. We develop a novel adaptive alternating-iteration algorithm to handle the L1 data-fitting term and to search the optimal parameters at the same time. Numerical examples are presented to demonstrate that the performance of the proposed algorithm is efficient, effective, and competitive in terms of visual quality and some criteria such as peak signal-to-noise ratio (PSNR), structure similarity (SSIM) [28], and spectral angle mapper (SAM) [19].

The outline of this paper is given as follows. In Section 2, we will give a detailed discussion of the proposed alternating-iteration algorithm for solving SVTV-L1 model automatically. The numerical experiments are given in Section 3 to demonstrate the effectiveness of the proposed algorithm. Finally, some concluding remarks are given in Section 4.

2. The Proposed Adaptive Algorithm

2.1. The formulation

We consider the following SVTV-L1 model for color image restoration in this paper:

$$\min_{\mathbf{u}} \lambda\,\mathrm{SVTV}(\mathbf{u}) + \|\mathbf{K}\mathbf{u}-\mathbf{f}\|_1, \tag{2.1}$$

where

$$\mathrm{SVTV}(\mathbf{u}) = \sum_{i=1}^{m}\sum_{j=1}^{n} \sqrt{|(\mathbf{D}_x\mathbf{u})_{ij}|_s^2 + |(\mathbf{D}_y\mathbf{u})_{ij}|_s^2} + \alpha\sqrt{|(\mathbf{D}_x\mathbf{u})_{ij}|_v^2 + |(\mathbf{D}_y\mathbf{u})_{ij}|_v^2}.$$

λ, α are positive parameters to control the regularization term and the value term respectively. $\mathbf{D}_x, \mathbf{D}_y$ are the difference operators in the x, y directions, and $|\cdot|_s, |\cdot|_v$ are the saturation norm, value norm given as follows:

$$
\begin{aligned}
&(\mathbf{D}_x\mathbf{u})_{ij} = \mathbf{u}(i,j) - \mathbf{u}(i-1,j), \quad (\mathbf{D}_y\mathbf{u})_{ij} = \mathbf{u}(i,j) - \mathbf{u}(i,j-1),\\
&|(\mathbf{D}_x\mathbf{u})_{ij}|_s = \frac{1}{3}\|W(\mathbf{D}_x\mathbf{u})_{ij}\|, \qquad |(\mathbf{D}_y\mathbf{u})_{ij}|_s = \frac{1}{3}\|W(\mathbf{D}_y\mathbf{u})_{ij}\|,\\
&|(\mathbf{D}_x\mathbf{u})_{ij}|_v = \frac{1}{\sqrt{3}}|(\mathbf{D}_x\boldsymbol{u}_1)_{ij} + (\mathbf{D}_x\boldsymbol{u}_2)_{ij} + (\mathbf{D}_x\boldsymbol{u}_3)_{ij}|,\\
&|(\mathbf{D}_y\mathbf{u})_{ij}|_v = \frac{1}{\sqrt{3}}|(\mathbf{D}_y\boldsymbol{u}_1)_{ij} + (\mathbf{D}_y\boldsymbol{u}_2)_{ij} + (\mathbf{D}_y\boldsymbol{u}_3)_{ij}|,
\end{aligned}
$$

where

$$
W = \begin{bmatrix} 2 & -1 & -1 \\ -1 & 2 & -1 \\ -1 & -1 & 2 \end{bmatrix}.
$$

We then introduce an auxiliary variable $\boldsymbol{\eta}$ and derive the equivalent constrained form of (2.1),

$$
\begin{aligned}
&\min_{\mathbf{u},\boldsymbol{\eta}} \lambda\,\mathrm{SVTV}(\mathbf{u}) + \|\boldsymbol{\eta}\|_1\\
&\text{s.t.} \quad \boldsymbol{\eta} = \mathbf{K}\mathbf{u} - \mathbf{f}.
\end{aligned} \tag{2.2}
$$

Numerically, we consider the following unconstrained version of (2.2):

$$
\min_{\mathbf{u},\boldsymbol{\eta}} \lambda\,\mathrm{SVTV}(\mathbf{u}) + \|\boldsymbol{\eta}\|_1 + \frac{\beta_1}{2}\|\boldsymbol{\eta} - (\mathbf{K}\mathbf{u} - \mathbf{f})\|^2, \tag{2.3}
$$

where β_1 is a penalty parameter. We then make use of alternating iteration to solve problem (2.3), and we summarize it in the Algorithm 2.1.

Algorithm 2.1: Main Algorithm**.**

1 Give the degraded image $\mathbf{f}$, parameter β_1, θ, stopping criterion ϵ_1.
2 Initialize $\mathbf{u}^0$ by setting $\mathbf{u}^0 = \mathbf{f}$.
3 For fixed $\mathbf{u}^k$, update $\boldsymbol{\eta}^{k+1}$ by solving

$$
\min_{\boldsymbol{\eta}} \|\boldsymbol{\eta}\|_1 + \frac{\beta_1}{2}\|\boldsymbol{\eta} - (\mathbf{K}\mathbf{u}^k - \mathbf{f})\|^2. \tag{2.4}
$$

4 For fixed $\mathbf{u}^k, \boldsymbol{\eta}^{k+1}$, update $\mathbf{u}^{k+1}$ by solving

$$
\min_{\mathbf{u}} \lambda\,\mathrm{SVTV}(\mathbf{u}) + \frac{\beta_1}{2}\|\boldsymbol{\eta}^{k+1} - (\mathbf{K}\mathbf{u} - \mathbf{f})\|^2. \tag{2.5}
$$

5 Increase β_1 by using $\beta_1 = \theta \cdot \beta_1$.
6 Repeat Step 3 to 5 until $\|(\mathbf{u}_3)^{k+1} - (\mathbf{u}_3)^k\|_2 / \|(\mathbf{u}_3)^k\|_2 \le \epsilon_1$.

2.2. The subproblems

The subproblem 2.4 has a closed-form solution by using soft-thresholding operation,

$$
\boldsymbol{\eta} = \max\left\{|\mathbf{K}\mathbf{u}^k - \mathbf{f}| - \frac{1}{\beta_1}, 0\right\} \cdot \frac{\mathbf{K}\mathbf{u}^k - \mathbf{f}}{|\mathbf{K}\mathbf{u}^k - \mathbf{f}|}. \tag{2.6}
$$

We then focus on solving the subproblem (2.5). We first note that the proposed minimization problem (2.5) is equivalent to

$$\min_{\mathbf{u}} \mathrm{SVTV}(\mathbf{u}) + \frac{\beta_1}{2\lambda}\|\mathbf{K}\mathbf{u} - \mathbf{f} - \boldsymbol{\eta}^{k+1}\|^2. \tag{2.7}$$

Remark that the above optimization problem is not linear least squares problem, and the generalized cross validation cannot be applied directly for estimation of regularization parameter. Therefore, we introduce an auxiliary variable $\hat{\mathbf{u}}$ and an additional quadratic term to get an equivalent version of (2.7)

$$\min_{\mathbf{u},\hat{\mathbf{u}}} \mathrm{SVTV}(\hat{\mathbf{u}}) + \frac{\beta_1}{2\lambda}\|\mathbf{K}\mathbf{u} - \mathbf{f} - \boldsymbol{\eta}^{k+1}\|^2 + \frac{\beta_2}{2}\|\mathbf{u} - \hat{\mathbf{u}}\|^2. \tag{2.8}$$

Note that as β_2 increases, the solution of problem (2.8) will get closer to that of problem (2.7). Therefore, the value of β_2 will be increased iteration by iteration in practice. Algorithm 2.2 is summarized for solving (2.8).

Algorithm 2.2: GCV Algorithm**.**

1 Give the degraded image $\mathbf{f}$, parameter β_2, θ, stopping criterion ϵ_2.
2 Initialize $\mathbf{u}_0$ by setting $\mathbf{u}_0 = \mathbf{u}^k$.
3 For fixed $\mathbf{u}_j$, compute $\hat{\mathbf{u}}_{j+1}$ by solving

$$\min_{\hat{\mathbf{u}}} \mathrm{SVTV}(\hat{\mathbf{u}}) + \frac{\beta_2}{2}\|\mathbf{u}_j - \hat{\mathbf{u}}\|^2. \tag{2.9}$$

4 For fixed $\hat{\mathbf{u}}_{j+1}, \boldsymbol{\eta}^{k+1}$, estimate parameter $\hat{\lambda}$ $(\lambda\beta_2/\beta_1)$ by solving

$$\hat{\lambda} = \arg\min_{\lambda} \frac{\sum_{i=1}^{mn}\big[\lambda/\big(\alpha_i^2+\lambda\big)\big]^2\big[\mathcal{F}\big(\mathbf{f}+\boldsymbol{\eta}^{k+1}-\mathbf{K}\hat{\mathbf{u}}_{j+1}\big)\big]_i^2}{\big[\sum_{i=1}^{mn}\lambda/\big(\alpha_i^2+\lambda\big)\big]^2}, \tag{2.10}$$

where α_i refers to the eigenvalues of $\mathbf{K}$.
5 For fixed $\hat{\mathbf{u}}_{j+1}, \boldsymbol{\eta}^{k+1}$, compute $\mathbf{u}_{j+1}$ by solving

$$\min_{\mathbf{u}} \frac{\beta_1}{2\lambda}\|\mathbf{K}\mathbf{u} - \mathbf{f} - \boldsymbol{\eta}^{k+1}\|^2 + \frac{\beta_2}{2}\|\mathbf{u} - \hat{\mathbf{u}}_{j+1}\|^2,$$

which is equivalent to

$$\min_{\mathbf{u}} \|\mathbf{K}\mathbf{u} - \mathbf{f} - \boldsymbol{\eta}^{k+1}\|^2 + \hat{\lambda}\|\mathbf{u} - \hat{\mathbf{u}}_{j+1}\|^2. \tag{2.11}$$

6 Increase β_2 by using $\beta_2 = \theta \cdot \beta_2$.
7 Repeat Step 3 to 6 until $\|(\mathbf{u}_3)_{j+1} - (\mathbf{u}_3)_j\|_2/\|(\mathbf{u}_3)_j\|_2 \le \epsilon_2$.

Subproblem (2.9) is a SVTV-L2 minimization problem, and can be solved by using alternating direction method of multipliers (ADMM) iteration, see details in [16]. Note that (2.11) is a linear least squares problem, and the associated parameter $\hat{\lambda}$ can be estimated by using the generalized cross validation technique which will be discussed in Section 2.3. The estimating problem (2.10) can be effectively solved by using line searching methods such as golden section

searching. Subproblem (2.11) can be solved by using fast Fourier transforms [14]. To be more specific, $\mathbf{u}_{j+1}$ can be computed as follows:

$$\mathbf{u}_{j+1} = \frac{\mathcal{F}(\mathbf{K})^* \circ \mathcal{F}\big(\mathbf{f} + \boldsymbol{\eta}^{k+1} - \mathbf{K}\hat{\mathbf{u}}_{j+1}\big)}{\hat{\lambda} + \mathcal{F}(\mathbf{K})^* \circ \mathcal{F}(\mathbf{K})} + \hat{\mathbf{u}}_{j+1}.$$

2.3. The estimation of $\hat{\lambda}$ by using GCV

The method of regularization is used to achieve stability for restoration problem. Choosing a proper parameter is an essential yet complex problem for variational methods. In this subsection, we will briefly introduce the method of generalized cross-validation and its application in our proposed algorithm. Recall the classical Tikhonov regularization [10], a regularization operator $\mathcal{D}$ is added to restrict the set of the admissible solution. Then the regularized solution $u(\lambda)$ is computed as follows:

$$\min_{u(\lambda)}\{\lambda\|\mathcal{D}u(\lambda)\|^2 + \|\mathcal{K}u(\lambda) - f\|^2\},$$

where $\mathcal{K}$ is a degradation kernel. The solution of the above problem can be derived by solving the following equation:

$$(\lambda\mathcal{D}^\top\mathcal{D} + \mathcal{K}^\top\mathcal{K})u(\lambda) = \mathcal{K}^\top u(\lambda).$$

For different choices of $\mathcal{D}$ and $\mathcal{K}$ with some appropriate boundary conditions, one can find some fast algorithms to deal with the above equation, see [15] for detailed discussion.

If the image is flattened to an mn-dimensional vector, we can quickly select the parameter λ by using the GCV method. GCV is a method that estimates λ without requiring an estimate of the noise variance. It is based on the concept of prediction errors. Let u_λ^k be the vector that minimizes the following error:

$$\lambda\|\mathcal{D}u(\lambda)\|^2 + \sum_{i\neq k}\big([\mathcal{K}u(\lambda)]_i - [f]_i\big)^2,$$

where $[\mathcal{K}u(\lambda)]_i$ and $[f]_i$ are the i-th element of $\mathcal{K}u(\lambda)$ and f respectively. If parameter λ is chosen such that u_λ^k is a good estimate of u, then $[\mathcal{K}u_\lambda^k]_k$ should be a good approximation of $[f]_k$ on average. For a given λ and solution u_λ^k, the mean squared error between the predicted value $[\mathcal{K}u_\lambda^k]_k$ and the actual value $[f]_k$ is defined as following:

$$\frac{1}{mn}\sum_{k=1}^{n}\big([\mathcal{K}u_\lambda^k]_k - [f]_k\big)^2.$$

GCV method is proposed to minimize the weighted version of the above error

$$\min_\lambda V(\lambda) = \min_\lambda \frac{1}{mn}\sum_{k=1}^{n}\big[\mathcal{K}u_\lambda^k\big]_k - ([f]_k)^2\left[\frac{1 - a_{kk}(\lambda)}{1 - \sum_{j=1}^{mn}a_{jj}(\lambda)/mn}\right]^2,$$

where $a_{jj}(\lambda)$ is the (j,j)-th entry of the following matrix:

$$A(\lambda) = \mathcal{K}(\mathcal{K}^\top\mathcal{K} + \lambda\mathcal{D}^\top\mathcal{D})^{-1}\mathcal{K}^\top.$$

If the periodic boundary condition or the Neumann boundary condition is used for both $\mathcal{K}$ and $\mathcal{D}^\top\mathcal{D}$, we can rewrite $V(\lambda)$ as follows:

$$V(\lambda) = n\frac{\sum_{i=1}^{n}\big[\lambda\beta_i/\big(\alpha_i^2 + \lambda\beta_i\big)\big]^2[\mathcal{F}f]_i^2}{\big[\sum_{i=1}^{n}\lambda\beta_i/\big(\alpha_i^2 + \lambda\beta_i\big)\big]^2}, \tag{2.12}$$

where $\mathcal{F}$ represents either the discrete Fourier matrix or the discrete cosine transform matrix, and α_i and β_i represent the eigenvalues of $\mathcal{K}$ and $\mathcal{D}^\top\mathcal{D}$ respectively, see [26] for detailed discussion. Then we can solve the problem of parameter selection in SVTV-L1 model. For subproblem (2.10), let $\mathbf{v} = \mathbf{u} - \hat{\mathbf{u}}$, (2.11) can be rewritten as

$$\min_{\mathbf{v}} \|\mathbf{K}\mathbf{v} + \mathbf{K}\hat{\mathbf{u}} - \mathbf{f} - \boldsymbol{\eta}^{k+1}\|^2 + \hat{\lambda}\|\mathbf{v}\|^2,$$

which is a linear least squares problem with Tikhonov regularization, and therefore the associated regularization parameter $\hat{\lambda}$ can be estimated by the generalized cross validation technique which has been discussed above. To be more specific, suppose $\mathbf{u} \in \mathbb{R}^{m\times n\times c}$, and regard each channel of $\mathbf{u}$ as an $mn \times 1$ vector, and $\mathcal{D} = \mathbf{I}, \mathcal{K} = \mathbf{K}, f = \mathbf{K}\hat{\mathbf{u}} - \mathbf{f} - \boldsymbol{\eta}^{k+1}$, which means α_i refers to the eigenvalues of $\mathbf{K}$, and β_i refers to the eigenvalues of $\mathbf{I}$, i.e. $\beta_i = 1$. Then we can estimate $\hat{\lambda}$ by minimizing the rewritten version of (2.12)

$$\hat{\lambda} = \arg\min_{\lambda} \frac{\sum_{i=1}^{mn} \left[\lambda/\left(\alpha_i^2 + \lambda\right)\right]^2 \left[\mathcal{F}\left(\mathbf{f} + \boldsymbol{\eta}^{k+1} - \mathbf{K}\hat{\mathbf{u}}_{j+1}\right)\right]_i^2}{\left[\sum_{i=1}^{mn} \lambda/\left(\alpha_i^2 + \lambda\right)\right]^2}.$$

3. Numerical Experiments

To demonstrate the effectiveness of the proposed algorithm, we present the numerical results in this section. We compare CTV [9], HTV [20], Framelet [8], SVTV-L1 [27] and the proposed adaptive SVTV-L1 model (ASVTV-L1) for image restoration on several testing images. The quality of the recovered images is measured by the peak signal to noise ratio, the structure similarity [28], which has been proven to be consistent with human eye perception, and the spectral angle mapper [19], which is used for measuring the similarity between two spectra.

For the stopping criteria, we break the iterations when the relative error of the successive iterates is less than or equal to 1×10^{-6} for all the testing methods. For the proposed ASVTV model, we set the stopping criterion $\epsilon_2 = 1 \times 10^{-4}$. The initial value of β_2 is set to be 0.01 and the value of β_2 at each inner iteration is increased by a factor of $\theta = 1.05$ so that β_2 becomes larger. For outer iteration, we set the stopping criterion $\epsilon_1 = 1 \times 10^{-6}$. The initial value of β_1 is set to be 0.01 and the value of β_1 at each inner iteration is increased by a factor of $\theta = 1.05$ so that β_1 becomes larger. For the SVTV model (2.9), we set the parameter of the value channel to be $\alpha = 0.1$. For the parameter of the fidelity term (λ) in SVTV model, we set a range in between $[\sqrt{N}/1000, \sqrt{N}/10]$ (N is the total pixel numbers) with a step size of 0.5 and choose the optimal values in terms of PSNR. The range of fidelity parameter for CTV model and Framelet model is also set to be $[\sqrt{N}/1000, \sqrt{N}/10]$. For HTV model, we set $c \in \{0.1, 0.2\}$, $\beta_1 = 15, \beta_2 = 40, \beta_3 \in \{100, 200\}$ for all the experiments. For SVTV, CTV and Framelet models, we set the penalty parameter $\beta \in \{0.01, 0.1\}$ for iterations when the ADMM method is employed.

3.1. Image denoising: Poisson noise

In this subsection, we test the denoising effect of the proposed model. In order to test the proposed model with respect to different noise levels, we make use of the following Matlab command to generate the degraded image contaminated by Poisson noise:

$$\mathbf{u}_{\text{noisy}} = d * \texttt{poissrnd}\big(\max(0, \mathbf{u}/d)\big),$$

where d refers to the scale of Possion noise.

We make use of 50 images taken from the Berkeley Segmentation Dataset [21] to test the proposed model for image denoising with respect to different noise levels. The ground-truth images are degraded artificially by Poisson noise with scales of $d = 0.1, 0.2, 0.3$. By choosing the optimal values of the regularization parameter in terms of PSNR for each testing method, we compute the SSIM and PSNR values of the restored results. In order to show the preservation of colors, we also compute the mean value of the spectral angle mapper of all pixels corresponding to the restored results and noise-free images. We show the relative error (in percentage) of the noisy images by using the ratio of the L2-norm of the difference between noisy and noise-free image to the L2-norm of the noise-free image in the following denoising experiments:

$$\text{Error} = \|\mathbf{u} - \mathbf{u}_{\text{noisy}}\|_2 / \|\mathbf{u}\|_2.$$

In Figs. 3.1-3.3, we show the spatial distributions of the SSIM, PSNR, and SAM values of the restored results by using different methods corresponding to Poisson noise of $d = 0.1, 0.2, 0.3$ respectively. We also report the average values of 50 testing images in Table 3.1 (The best values are in bold). We see from the measure values that the proposed ASVTV-L1 model is very competitive in terms of SSIM, PSNR, and SAM criterion. Meanwhile, note that the proposed ASVTV-L1 model is an unsupervised method with respect to parameters, while the other testing methods are supervised. Therefore, the proposed ASVTV-L1 model is both efficient and effective for poisson noise removing in terms of the above discussion.

As examples, we show some experimental results and display the corresponding zooming parts of the restored results in Figs. 3.4-3.9. We see from the results that the restored images by using the proposed ASVTV-L1 model is significantly better than those by using CTV, HTV and Framelet visually, especially in eliminating color artifacts caused by Poisson noise. Recall that SVTV-L1 model is also good at removing color artifacts, however, the proposed ASVTV-L1 model has better color preservation, see especially the zooming parts in Figs. 3.5 and 3.7.

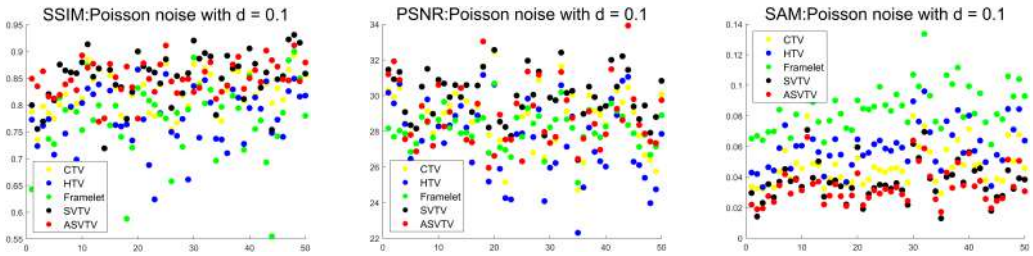

Fig. 3.1. The spatial distributions of SSIM, PSNR, and SAM values of 50 images with noise intensity of 0.1.

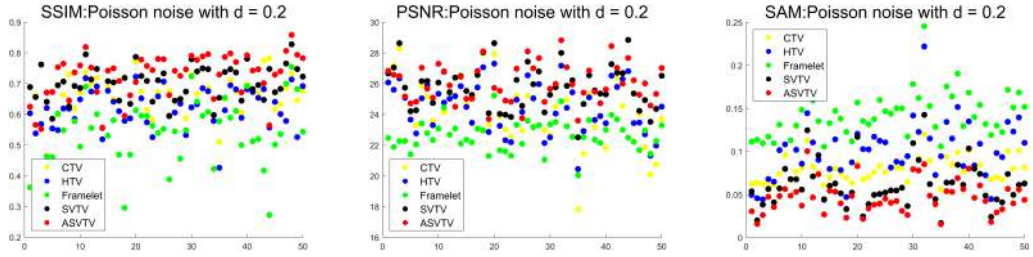

Fig. 3.2. The spatial distributions of SSIM, PSNR, and SAM values of 50 images with noise intensity of 0.2.

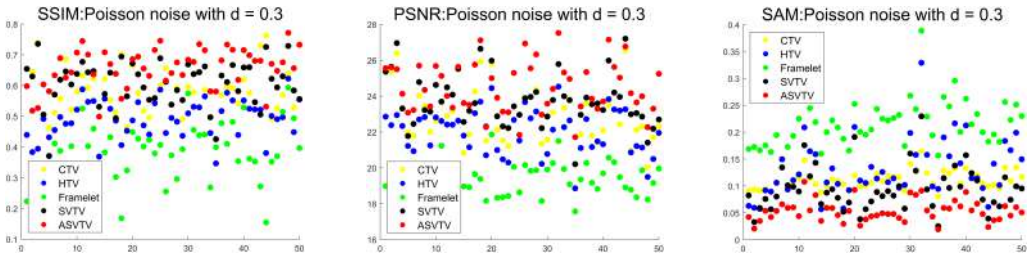

Fig. 3.3. The spatial distributions of SSIM, PSNR, and SAM values of 50 images with noise intensity of 0.3.

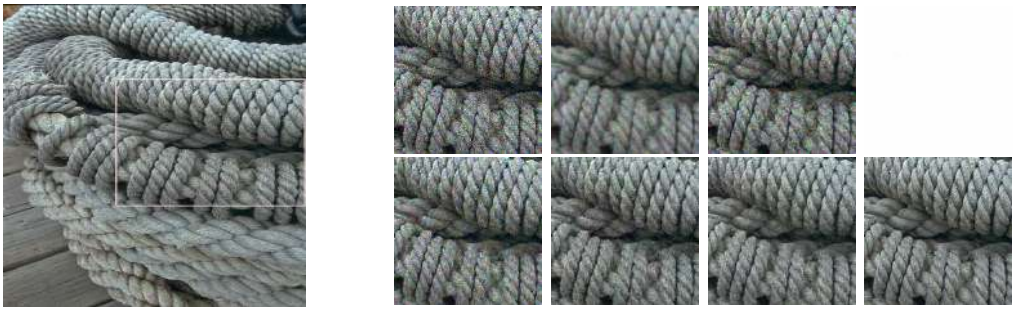

Fig. 3.4. Left: the ground-truth image; Right (the zooming parts): the first row: the Poisson noisy image with $d = 0.2$, restored results by using CTV and HTV respectively; the second row: restored results by using Framelet, SVTV, ASVTV and the ground-truth image respectively.

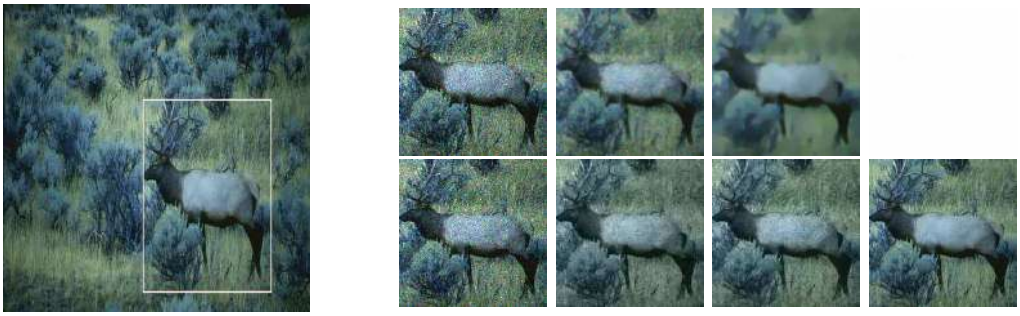

Fig. 3.5. Left: the ground-truth image; Right (the zooming parts): the first row: the Poisson noisy image with $d = 0.2$, restored results by using CTV and HTV respectively; the second row: restored results by using Framelet, SVTV, ASVTV and the ground-truth image respectively.

We report the SSIM, PSNR, and SAM values in Table 3.1, and we can clearly observe that the proposed ASVTV-L1 model outperforms other testing methods.

3.2. Image denoising: Mixed noise

In this subsection, we test the performance of the proposed algorithm for mixed noise removal. We first add Poisson noise with $d = 0.1$, and then add Gaussian noise with standard deviation $\sigma = 0.05$ to the ground-truth images. Again by selecting the optimal value of the regularization parameter of each method, we calculate the SSIM, PSNR, and SAM values of the restored results and show the spatial distribution of SSIM, PSNR, and SAM values of each

Table 3.1: The SSIM, PSNR, and SAM values of the restored results corresponding to different methods.

Level	$d = 0.1$					
	Average				Error(%)	1.65
Measure	Noisy	ASVTV	SVTV	CTV	HTV	Framelet
SSIM	0.6290	0.8490	**0.8510**	0.8214	0.7722	0.7623
PSNR	24.3432	28.8184	**29.9704**	28.7011	27.4917	28.1111
SAM	0.1209	**0.0339**	0.0369	0.0469	0.0602	0.0862
Level	$d = 0.2$					
	Average				Error(%)	3.34
Measure	Noisy	ASVTV	SVTV	CTV	HTV	Framelet
SSIM	0.3764	**0.7247**	0.6980	0.6672	0.6200	0.5302
PSNR	18.4764	**26.0025**	25.7897	24.5879	24.4666	22.6535
SAM	0.2397	**0.0470**	0.0614	0.0792	0.0989	0.1433
	Fig. 3.4				Error(%)	2.91
Measure	Noisy	ASVTV	SVTV	CTV	HTV	Framelet
SSIM	0.4339	**0.7781**	0.7394	0.6739	0.5625	0.6014
PSNR	17.5695	**25.5387**	24.7184	23.8796	20.4497	21.6530
SAM	0.2264	**0.0217**	0.0233	0.0679	0.1546	0.1320
	Fig. 3.5				Error(%)	3.31
Measure	Noisy	ASVTV	SVTV	CTV	HTV	Framelet
SSIM	0.3815	**0.7417**	0.7031	0.6437	0.6056	0.5445
PSNR	18.7657	**27.0016**	26.3678	25.9584	25.0462	23.1724
SAM	0.2431	**0.0489**	0.0598	0.0811	0.050	0.2095
	Fig. 3.6				Error(%)	3.40
Measure	Noisy	ASVTV	SVTV	CTV	HTV	Framelet
SSIM	0.5605	**0.7937**	0.7746	0.6458	0.6189	0.6816
PSNR	18.7023	**25.3380**	24.6628	22.5623	20.6923	22.2659
SAM	0.2681	**0.0515**	0.0547	0.1669	0.1985	0.1659
Level	$d = 0.3$					
	Average				Error(%)	5.08
Measure	Noisy	ASVTV	SVTV	CTV	HTV	Framelet
SSIM	0.2472	**0.6550**	0.6339	0.5787	0.5206	0.5313
PSNR	15.1889	**24.5013**	23.6665	22.9241	22.0676	21.6161
SAM	0.3556	**0.0534**	0.0944	0.1116	0.1305	0.2180
	Fig. 3.7				Error(%)	4.25
Measure	Noisy	ASVTV	SVTV	CTV	HTV	Framelet
SSIM	0.2805	**0.6940**	0.6373	0.5760	0.5460	0.4271
PSNR	14.3376	**23.9104**	22.8787	21.5353	20.9927	18.3372
SAM	0.3316	**0.0239**	0.0313	0.1113	0.1593	0.2011
	Fig. 3.8				Error(%)	5.07
Measure	Noisy	ASVTV	SVTV	CTV	HTV	Framelet
SSIM	0.2305	**0.6406**	0.6218	0.5382	0.4948	0.3732
PSNR	15.3402	**25.5523**	24.9387	23.9595	22.7603	19.8367
SAM	0.3589	**0.0506**	0.0604	0.1162	0.0650	0.3231
	Fig. 3.9				Error(%)	5.04
Measure	Noisy	ASVTV	SVTV	CTV	HTV	Framelet
SSIM	0.3875	**0.6565**	0.5844	0.4482	0.4486	0.4936
PSNR	15.3383	**23.3014**	22.1798	21.7084	20.4980	19.1587
SAM	0.3988	**0.0645**	0.0840	0.1585	0.2124	0.2449

Fig. 3.6. Left: the ground-truth image; Right (the zooming parts): the first row: the Poisson noisy image with $d = 0.2$, restored results by using CTV and HTV respectively; the second row: restored results by using Framelet, SVTV, ASVTV and the ground-truth image respectively.

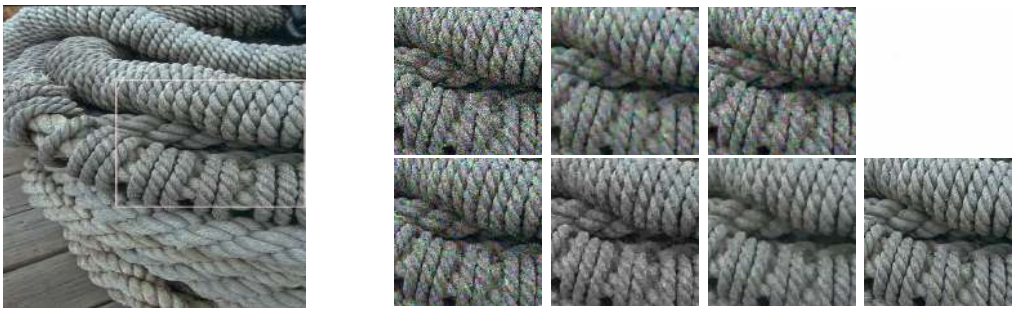

Fig. 3.7. Left: the ground-truth image; Right (the zooming parts): the first row: the Poisson noisy image with $d = 0.3$, restored results by using CTV and HTV respectively; the second row: restored results by using Framelet, SVTV, ASVTV and the ground-truth image respectively.

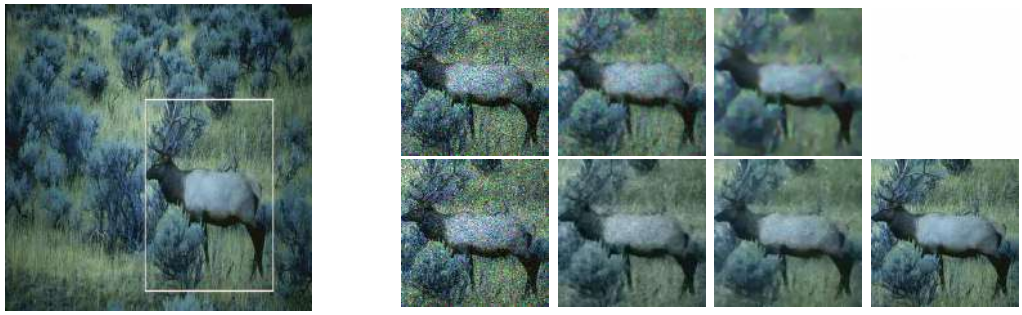

Fig. 3.8. Left: the ground-truth image; Right (the zooming parts): the first row: the Poisson noisy image with $d = 0.3$, restored results by using CTV and HTV respectively; the second row: restored results by using Framelet, SVTV, ASVTV and the ground-truth image respectively.

method in Fig 3.10. Again we see from the results that the proposed ASVTV-L1 algorithm is very competitive.

As examples of the experiment, we show some restored results of the noisy images by using different methods and the corresponding zoom-parts in Figs. 3.11-3.13 respectively. Again we see from the results that the proposed method is better than other testing methods in terms of visual quality. We also report the SSIM, PSNR, and SAM values in Table 3.2, and we can clearly observe that the proposed ASVTV-L1 model outperforms other testing methods.

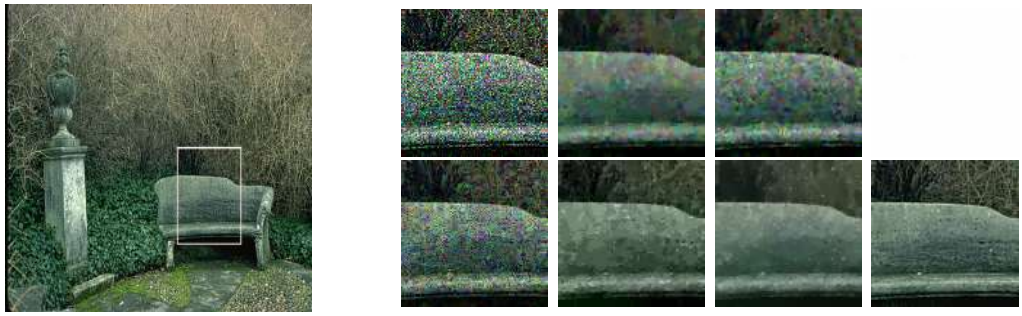

Fig. 3.9. Left: the ground-truth image; Right (the zooming parts): the first row: the Poisson noisy image with $d = 0.3$, restored results by using CTV and HTV respectively; the second row: restored results by using Framelet, SVTV, ASVTV and the ground-truth image respectively.

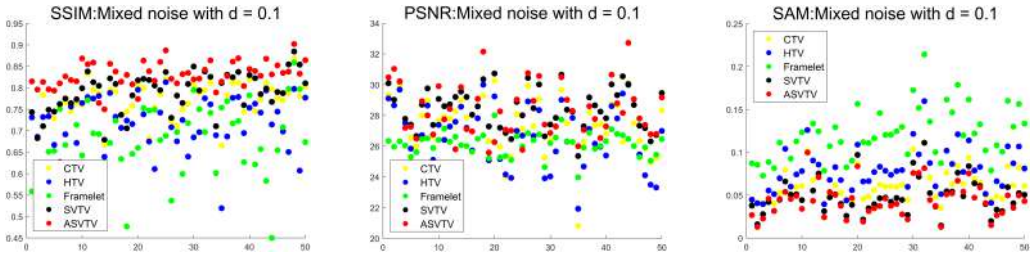

Fig. 3.10. The spatial distributions of SSIM, PSNR, and SAM values of 50 images with mixed noise.

Table 3.2: The SSIM, PSNR, and SAM values of the restored results corresponding to different methods.

Level	Mixed					
	Average				Error(%)	2.13
Measure	Noisy	ASVTV	SVTV	CTV	HTV	Framelet
SSIM	0.5151	**0.8302**	0.7906	0.7688	0.7185	0.6711
PSNR	22.1576	28.2501	**28.4882**	27.4495	26.6442	26.1488
SAM	0.1747	**0.0444**	0.0494	0.0615	0.0778	0.1232
	Fig. 3.11				Error(%)	2.79
Measure	Noisy	ASVTV	SVTV	CTV	HTV	Framelet
SSIM	0.6290	**0.8683**	0.7756	0.7430	0.6477	0.6081
PSNR	22.3127	**29.8982**	28.8184	28.2284	24.6719	25.3711
SAM	0.2289	**0.0393**	0.0402	0.0632	0.0482	0.1103
	Fig. 3.12				Error(%)	2.69
Measure	Noisy	ASVTV	SVTV	CTV	HTV	Framelet
SSIM	0.2705	**0.8300**	0.7980	0.7541	0.7367	0.4109
PSNR	21.9159	**32.1482**	29.4081	29.3102	29.0727	25.3816
SAM	0.1959	0.0239	0.0240	0.0521	**0.0219**	0.0957
	Fig. 3.13				Error(%)	1.81
Measure	Noisy	ASVTV	SVTV	CTV	HTV	Framelet
SSIM	0.6416	**0.8166**	0.7426	0.6964	0.6302	0.6654
PSNR	21.5432	**27.0188**	25.4377	23.3002	21.8360	23.4001
SAM	0.1539	**0.0390**	0.0403	0.0728	0.0962	0.0959

Fig. 3.11. Left: the ground-truth image; Right (the zooming parts): the first row: the mixed noisy image with $d = 0.1, \sigma = 0.05$, restored results by using CTV and HTV respectively; the second row: restored results by using Framelet, SVTV, ASVTV and the ground-truth image respectively.

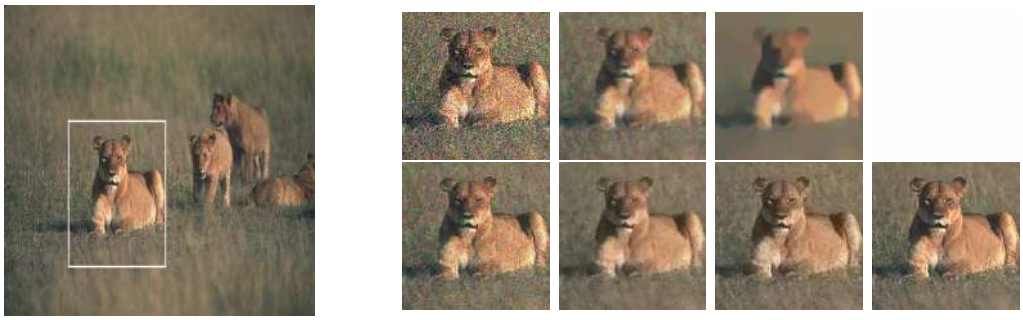

Fig. 3.12. Left: the ground-truth image; Right (the zooming parts): the first row: the mixed noisy image with $d = 0.1, \sigma = 0.05$, restored results by using CTV and HTV respectively; the second row: restored results by using Framelet, SVTV, ASVTV and the ground-truth image respectively.

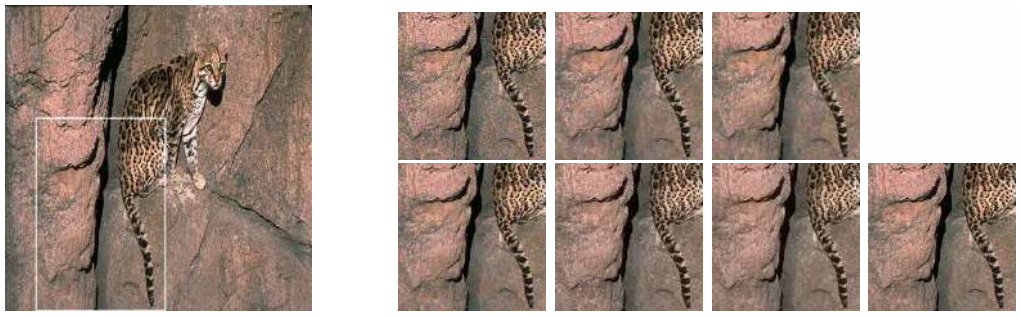

Fig. 3.13. Left: the ground-truth image; Right (the zooming parts): the first row: the mixed noisy image with $d = 0.1, \sigma = 0.05$, restored results by using CTV and HTV respectively; the second row: restored results by using Framelet, SVTV, ASVTV and the ground-truth image respectively.

3.3. Comparison with SVTV-L1

Noting that SVTV-L1 and ASVTV-L1 share the advantages of effective color-disturbance removal created by SVTV regularization. In this subsection, we further compare SVTV-L1 and ASVTV-L1 based on our numerical experiments. Recall that 50 ground-truth images are degraded with Poisson noise of $d = 0.1, 0.2, 0.3$ and Poisson-Gaussian mixed noise (Poisson noise of $d = 0.1$ and Gaussian noise of standard deviation $\sigma = 0.05$).

The average SSIM, PSNR, and SAM values of 50 images are already reported in Table 3.1. We calculate the difference of SSIM, PSNR, and SAM values between ASVTV-L1 and SVTV-L1 (values of ASVTV-L1 minus values of SVTV-L1), and display the spatial distributions in Figs. 3.14-3.17. For PSNR and SSIM, the red dots above the X-axis indicate that ASVTV-L1 is better, otherwise SVTV-L1 is better. For SAM, the red dots below the X-axis indicate that ASVTV-L1 is better, otherwise SVTV-L1 is better. We can clearly see the advantages and disadvantages of the two methods through the scatter plots. Specifically, ASVTV-L1 is generally competitive compared with SVTV-L1 for Poisson noise of $d = 0.1$. As noise level increases, the advantages of ASVTV-L1 are more obvious in terms of SSIM, PSNR, and SAM values on all of the testing degraded images. Therefore, ASVTV-L1 outperforms SVTV-L1 in terms of visual quality and the measure values.

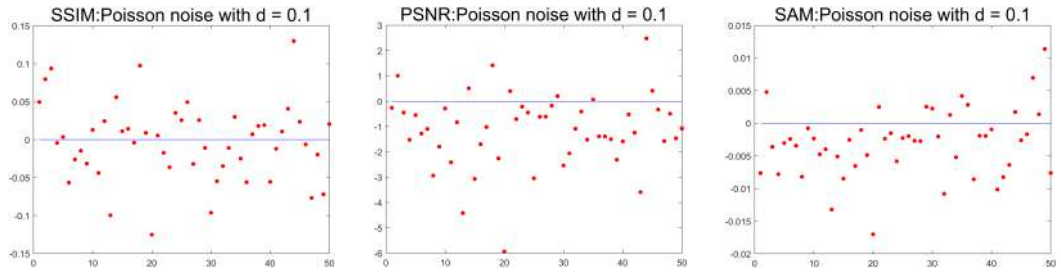

Fig. 3.14. The spatial distributions of the difference in SSIM, PSNR, and SAM between ASVTV-L1 and SVTV-L1 (Poisson noise $d = 0.1$).

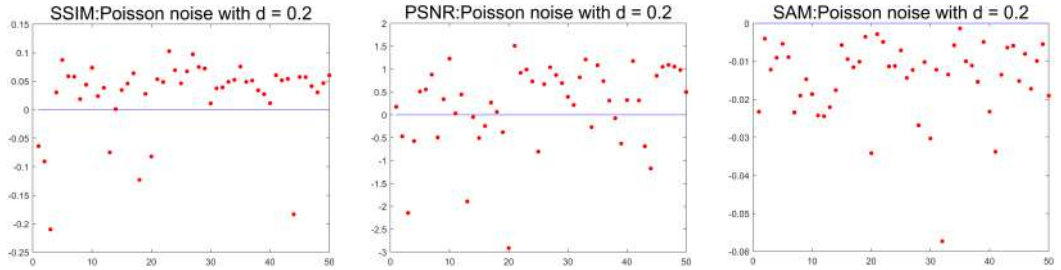

Fig. 3.15. The spatial distributions of the difference in SSIM, PSNR, and SAM between ASVTV-L1 and SVTV-L1 (Poisson noise $d = 0.2$).

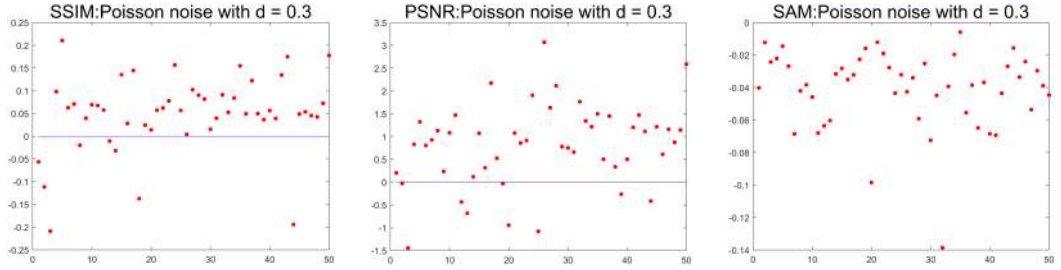

Fig. 3.16. The spatial distributions of the difference in SSIM, PSNR, and SAM between ASVTV-L1 and SVTV-L1 (Poisson noise $d = 0.3$).

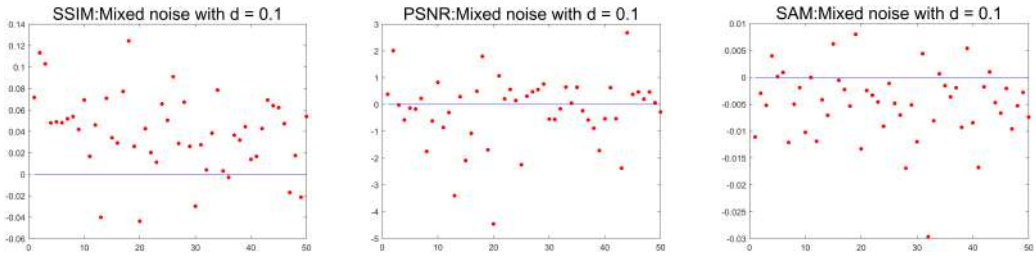

Fig. 3.17. The spatial distributions of the difference in SSIM, PSNR, and SAM between ASVTV-L1 and SVTV-L1 (Mixed noise).

4. Conclusion

As a summary, we have proposed an adaptive algorithm for L1-fidelity color image restoration by using saturation-value total variation in this paper. We make use of the generalized cross validation method efficiently and automatically to estimate the regularization parameter associated with the priors in SVTV-L1 model for color image restoration. We develop a novel adaptive alternating-iteration algorithm to handle the L1 data-fitting term and to search the optimal parameters at the same time. In order to demonstrate the performance of the proposed ASVTV-L1 model, we have conducted several numerical experiments on Poisson noise removal and Poisson-Gaussian mixed noise removal. The experimental results show that the performance of the proposed algorithm is efficient, effective, and competitive in terms of visual quality and some criteria such as peak signal-to-noise ratio, structure similarity, and spectral angle mapper.

Acknowledgements. The work is supported by the Natural Science Foundation of Shanghai (Grant No. 22ZR1465300).

References

[1] J.-F. Aujol, G. Gilboa, T. Chan, and S. Osher, Structure-texture image decomposition-modeling, algorithms, and parameter selection, *Int. J. Comput. Vision*, **67** (2006), 111–136.

[2] P. Blomgren and T.F. Chan, Color TV: Total variation methods for restoration of vector-valued images, *IEEE Trans. Image Process.*, **7** (1998), 304–309.

[3] X. Bresson and T.F. Chan, Fast dual minimization of the vectorial total variation norm and applications to color image processing, *Inverse Probl. Imaging*, **2** (2008), 455.

[4] J.-F. Cai, R.H. Chan, and Z. Shen, A framelet-based image inpainting algorithm, *Appl. Comput. Harmon. Anal.*, **24** (2008), 131–149.

[5] A. Chambolle and T. Pock, A first-order primal-dual algorithm for convex problems with applications to imaging, *J. Math. Imaging Vision*, **40** (2011), 120–145.

[6] T.F. Chan and S. Esedoglu, Aspects of total variation regularized $L1$ function approximation, *SIAM J. Appl. Math.*, **65** (2005), 1817–1837.

[7] J. Darbon, Total variation minimization with $L1$ data fidelity as a constrast invariant filter, in: *Proceddings of the 4th International Symposium on Image and signal Processing and Analysis*, IEEE, (2005), 221–226.

[8] B. Dong, H. Ji, J. Li, Z. Shen, and Y. Xu, Wavelet frame based blind image inpainting, *Appl. Comput. Harmon. Anal.*, **32** (2012), 268–279.

[9] J. Duran, M. Moeller, C. Sbert, and D. Cremers, Collaborative total variation: A general framework for vectorial TV models, *SIAM J. Imaging Sci.*, **9** (2016), 116–151.

[10] H.W. Engl, M. Hanke, and A. Neubauer, *Regularization of Inverse Problems*, in: *Mathematics and Its Applications*, Vol. 375, Springer, 1996.

[11] M. Gan, H.-T. Zhu, G.-Y. Chen, and C.P. Chen, Weighted generalized cross-validation-based regularization for broad learning system, *IEEE Trans. Cybern.*, **52** (2020), 4064–4072.

[12] G. H. Golub, M. Heath, and G. Wahba, Generalized cross-validation as a method for choosing a good ridge parameter, *Technometrics*, **21** (1979), 215–223.

[13] A. Haddad, Texture separation $BV - G$ and $BV - L^1$ models, *Multiscale Model. Simul.*, **6** (2007), 273–286.

[14] Y. Huang, M.K. Ng, and Y.-W. Wen, A fast total variation minimization method for image restoration, *Multiscale Model. Simul.*, **7** (2008), 774–795.

[15] A. K. Jain, *Fundamentals of Digital Image Processing*, Prentice-Hall, Inc., 1989.

[16] Z. Jia, M.K. Ng, and W. Wang, Color image restoration by saturation-value total variation, *SIAM J. Imaging Sci.*, **12** (2019), 972–1000.

[17] L. Jiang, J. Huang, X.-G. Lv, and J. Liu, Alternating direction method for the high-order total variation-based poisson noise removal problem, *Numer. Algorithms*, **69** (2015), 495–516.

[18] S. Kollem et al., Image denoising for magnetic resonance imaging medical images using improved generalized cross-validation based on the diffusivity function, *Int. J. Imaging Syst. Technol.*, **32** (2022), 1263–1285.

[19] F.A. Kruse et al., The spectral image processing system (SIPS) – interactive visualization and analysis of imaging spectrometer data, *Remote Sens. Environ.*, **44** (1993), 145–163.

[20] G. Liu, T.-Z. Huang, and J. Liu, High-order TVL1-based images restoration and spatially adapted regularization parameter selection, *Comput. Math. Appl.*, **67** (2014), 2015–2026.

[21] D. Martin, C. Fowlkes, D. Tal, and J. Malik, A database of human segmented natural images and its application to evaluating segmentation algorithms and measuring ecological statistics, in: *Proceedings Eighth IEEE International Conference on Computer Vision*, Vol. 2, IEEE, 2001, 416–423.

[22] N. Nguyen, P. Milanfar, and G. Golub, Efficient generalized cross-validation with applications to parametric image restoration and resolution enhancement, *IEEE Trans. Image Process.*, **10** (2001), 1299–1308.

[23] M. Nikolova, A variational approach to remove outliers and impulse noise, *J. Math. Imaging Vision*, **20** (2004), 99–120.

[24] Z. Shen, Wavelet frames and image restorations, in: *Proceedings of the International Congress of Mathematicians*, World Scientific, 2010, 2834–2863.

[25] D.N.H. Thanh, L.T. Thanh, N.N. Hien, and S. Prasath, Adaptive total variation L1 regularization for salt and pepper image denoising, *Optik*, **208** (2020), 163677.

[26] W. Wang and M. K. Ng, On algorithms for automatic deblurring from a single image, *J. Comput. Math*, **30** (2012), 80–100.

[27] W. Wang and Q. Song, Color image restoration based on saturation-value total variation plus L1 fidelity, *Inverse Problems*, **38** (2022), 085009.

[28] Z. Wang, A.C. Bovik, H.R. Sheikh, and E.P. Simoncelli, Image quality assessment: From error visibility to structural similarity, *IEEE Trans. Image Process.*, **13** (2004), 600–612.

[29] W. Yin, D. Goldfarb, and S. Osher, A comparison of three total variation based texture extraction models, *J. Visual Commun. Image Represent.*, **18** (2007), 240–252.

[30] B. Zhang, J.M. Fadili, and J.-L. Starck, Wavelets, ridgelets, and curvelets for Poisson noise removal, *IEEE Trans. Image Process.*, **17** (2008), 1093–1108.

[31] H. Zhang, Y. Dong, and Q. Fan, Wavelet frame based Poisson noise removal and image deblurring, *Signal Process.*, **137** (2017), 363–372.

[32] X. Zhang, M.K. Ng, and M. Bai, A fast algorithm for deconvolution and Poisson noise removal, *J. Sci. Comput.*, **75** (2018), 1535–1554.